Int. J. Solids Structures Vol. 19, No. 10, pp. 925–934, 1983
Printed in Great Britain.

0020-7683/83 $3.00 + .00

ELASTIC RESPONSE TO A TIME-HARMONIC TORSION-FORCE ACTING ON A BORE SURFACE†

R. PARNES
Department of Solid Mechanics, Materials and Structures, School of Engineering,
Tel-Aviv University, 69978 Tel-Aviv, Israel

(*Received* 12 *July* 1982)

Abstract—The response of an elastic medium to torsional line loads applied on the surface of a cylindrical cavity, and having a harmonic time-dependence, is studied. Integral representations of the stress and displacement fields are obtained and numerical results along a radial line emanating from the point of load applications and along the bore surface, are presented. The dynamic effect is represented by dynamic amplification factors and it is shown that, compared to the static case, the resulting outward radiating waves increase the effective radial penetration of the response.

1. INTRODUCTION

The application of tractions on the surface of a cylindrical cavity has been studied by several authors[1–6]. Westergaard[1] and later Tranter[2], studied the effect of static radial pressure loadings applied over a finite segment of a bore. Jordan[3] investigated the corresponding dynamic problem in 1962. The effect of a moving pressure line load was given by the author in [4] and later the corresponding problem for a torsional line load was studied in [5]. The response due to the application of static radial pressure and torsional line loads has recently been given in [6].

In the present investigation, we consider the steady-state problem of the effect of a torsional line load, with a harmonic time dependency, applied on the surface of a bore. This problem is of interest, e.g. in determining the displacements and stresses when a cylindrical inclusion with a tight fit is inserted in a medium by a twisting motion, resulting in a torsional frictional force at the interface. The results obtained can then be used as the Green's functions to determine the more complex displacement and stress patterns by superposition.

Numerical results are presented for the displacements and stress components along a radial line emanating from the point of load application and along the bore surface. The dynamic effect, as measured by dynamic amplification factors is studied and it is observed that greater radial penetration occurs, as compared to the static case, due to the radiation of outgoing S-waves in the medium. The solution to the present problem is also seen to degenerate to the static solution as the forcing frequency approaches zero.

2. GENERAL FORMULATION

Consider a cylindrical bore of radius $r = a$ in a linear elastic isotropic medium referred to a fixed non-dimensional coordinate system ($\rho = r/a$, θ, $\xi = z/a$) whose origin lies on the axis of the bore. A torsional line load, harmonic in time, with frequency $\omega = 2\pi f$, is applied uniformly along the circle at $z = 0$ (Fig. 1). The stresses on the boundary $\rho = 1$ are then given as

$$\sigma_{r\theta} = \frac{P}{a}\delta(\xi)\,e^{-i\omega t}, \qquad \sigma_{rr} = 0, \qquad \sigma_{rz} = 0 \tag{1}$$

where $\delta(\xi)$ is the Dirac-delta function.

†This work was initiated while the author was on leave at Laboratoire de Mécanique des Solides, Ecole Polytechnique, Palaiseau, France, during 1980–1981.

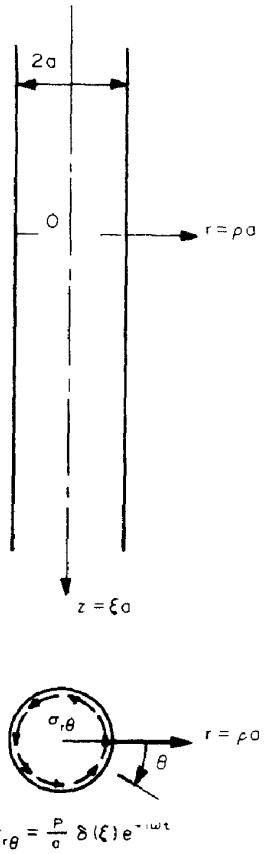

Fig. 1. Geometry of problem.

The displacement

$$\tilde{u}(\rho, \theta, \xi, t) = w\tilde{k}_r + v\tilde{k}_\theta + u\tilde{k}_z \tag{2}$$

must satisfy the equation of motion for the elastic medium,

$$\mu\nabla^2\tilde{u} + (\lambda + u)\nabla\nabla \cdot \tilde{u} = a^2\rho_D\ddot{\tilde{u}}, \tag{3}$$

where μ and λ are the Lamé constants, ρ_D is the mass density and where

$$\nabla \equiv \frac{\partial}{\partial\rho}\tilde{k}_r + \frac{1}{\rho}\frac{\partial}{\partial\theta}\tilde{k}_\theta + \frac{\partial}{\partial\xi}\tilde{k}_z. \tag{4}$$

For the axisymmetric case considered, solutions satisfying eqn (3) and the boundary conditions are

$$v = v(\rho, \xi, t), \qquad u = w = 0. \tag{5}$$

Equation (3) then reduces to the scalar equation

$$\nabla^2 v = \frac{a^2}{C_s^2}\frac{\partial^2 v}{\partial t^2} \tag{6}$$

where

$$C_s = \sqrt{(\mu/\rho_D)} \tag{7}$$

is the propagation velocity of shear waves in the medium.

Defining a non-dimensional time

$$\tau = C_s t/a, \tag{8}$$

the displacement $v = v(\rho, \xi, \tau)$ must satisfy eqn (6) which, written explicitly, becomes

$$\frac{\partial^2 v}{\partial \rho^2} + \frac{1}{\rho}\frac{\partial v}{\partial \rho} - \frac{v}{\rho^2} + \frac{\partial^2 v}{\partial \xi^2} = \frac{\partial^2 v}{\partial \tau^2}. \tag{9}$$

The corresponding boundary conditions are then

$$\sigma_{r\theta} = \frac{P}{a}\delta(\xi)\,e^{-i\Omega\tau}, \qquad \sigma_{rr} = \sigma_{rz} = 0; \qquad \rho = 1 \tag{10}$$

where

$$\Omega = \omega a/C_s. \tag{11}$$

The stresses, obtained from the stress–strain relations

$$\tilde{\sigma} = \frac{1}{a}\{\lambda \nabla \cdot \tilde{u} I + \mu[\nabla \tilde{u} + \tilde{u}\nabla]\} \tag{12}$$

become

$$\sigma_{r\theta} = \frac{\mu}{a}\left(\frac{\partial v}{\partial \rho} - \frac{v}{\rho}\right) \tag{13a}$$

$$\sigma_{\theta z} = \frac{\mu}{a}\frac{\partial v}{\partial \xi} \tag{13b}$$

$$\sigma_{rr} = \sigma_{\theta\theta} = \sigma_{rz} = \sigma_{zz} = 0.$$

The last two conditions of eqn (10) are identically satisfied while the remaining boundary condition is expressed as

$$\left.\frac{\partial v}{\partial \rho} - \frac{v}{\rho}\right|_{\rho=1} = \frac{P}{\mu}\delta(\xi)\,e^{-i\Omega\tau}. \tag{14}$$

3. GENERAL SOLUTION

Using the integral representation for the Dirac-delta function[7]

$$\delta(\xi) = \frac{1}{\pi}\int_0^\infty \cos \alpha\xi \, d\alpha, \tag{15}$$

the boundary condition, eqn (14), becomes

$$\left.\frac{\partial v}{\partial \rho} - \frac{v}{\rho}\right|_{\rho=1} = \frac{P}{\pi\mu}\int_0^\infty \cos \alpha\xi \, d\alpha \, e^{-i\Omega\tau} \tag{16}$$

Steady state solutions of the equation of motion, compatible with the condition of eqn (16) have the form

$$v_\alpha(\rho, \xi, \tau) = f(\rho)\cos \alpha\xi \, e^{-i\Omega\tau}. \tag{17}$$

Substituting in eqn (9) yields

$$\frac{\partial^2 f}{\partial \rho^2} + \frac{1}{\rho}\frac{\partial f}{\partial \rho} + (\beta^2 - 1/\rho^2)f = 0 \tag{18}$$

where

$$\beta^2 = \Omega^2 - \alpha^2. \tag{19}$$

Wave solutions of eqn (18) for outward propagating waves are

$$f(\rho) = CH_1^{(1)}(\beta\rho)$$

where $H_n^{(1)}$ is the Hankel function of order n.

Thus, since all solutions of the form

$$v_\alpha(\rho, \xi, \tau) = C(\alpha)H_1^{(1)}(\beta\rho)\cos\alpha\xi\ \mathrm{e}^{-i\Omega\tau} \tag{20}$$

satisfy eqn (9), (where $C(\alpha)$ denotes that the constant depends on the parameter α), the general solution is given by

$$v(\rho, \xi, \tau) = \int_0^\infty C(\alpha)H_1^{(1)}(\beta\rho)\cos\alpha\xi\ \mathrm{d}\alpha\ \mathrm{e}^{-i\Omega\tau}. \tag{21}$$

Substituting in eqn (16), and using the standard expressions for the derivatives of $H_n^{(1)}$ and the appropriate recursion relations[8], yields the constant

$$C(\alpha) = -\frac{P}{\mu\pi}\frac{1}{\beta H_2^{(1)}(\beta)} \tag{22}$$

and hence the displacement becomes

$$v(\rho, \xi, \tau) = -\frac{P}{\mu\pi}\int_0^\infty \frac{H_1^{(1)}(\beta\rho)}{\beta H_2^{(1)}(\beta)}\cos\alpha\xi\ \mathrm{d}\alpha\ \mathrm{e}^{-i\Omega\tau}. \tag{23}$$

It should now be noted that β, as defined by eqn (19) is real for $\alpha < \Omega$, while for $\alpha > \Omega$, β becomes imaginary. Noting that for $\alpha > \Omega$, the Hankel function is of an imaginary argument, it becomes appropriate to subdivide the range of integration into regions $\alpha < \Omega$ and $\alpha > \Omega$. This will be particularly useful in interpreting the subsequent results.

To this end, we recall the relation[8]

$$K_n(x) = \frac{\pi}{2}\mathrm{e}^{\frac{1}{2}(n+1)\pi i}H_n^{(1)}(ix). \tag{24}$$

Defining the non-dimensional parameter

$$\eta = \alpha/\Omega, \tag{25}$$

eqn (23) is written finally as

$$\frac{v\mu}{P} = -\frac{1}{\pi}\left[\int_0^1 \frac{H_1^{(1)}(\beta\rho)}{(1-\eta^2)^{1/2}H_2^{(1)}(\beta)}\cos(\Omega\xi\eta)\,\mathrm{d}\eta + \int_1^\infty \frac{K_1(\gamma\rho)}{(\eta^2-1)^{1/2}K_2(\gamma)}\cos(\Omega\xi\eta)\,\mathrm{d}\eta\right]\mathrm{e}^{-i\Omega\tau} \tag{26}$$

where now

$$\beta = \Omega(1-\eta^2)^{1/2}, \qquad \gamma = \Omega(\eta^2-1)^{1/2}. \tag{27a, b}$$

It is observed that while the first integral represents, in general, a complex quantity, the latter will always be real. Equation (13) yields the following expressions for the stress components:

$$\frac{\sigma_{r\theta}a}{P} = \frac{\Omega}{\pi}\left[\int_0^1 \frac{H_2^{(1)}(\beta\rho)}{H_2^{(1)}(\beta)}\cos(\Omega\xi\eta)\,d\eta + \int_1^\infty \frac{K_2(\gamma\rho)}{K_2(\gamma)}\cos(\Omega\xi\eta)\,d\eta\right]e^{-i\Omega\tau} \tag{28a}$$

$$\frac{\sigma_{\theta z}a}{P} = \frac{\Omega}{\pi}\left[\int_0^1 \frac{\eta H_1^{(1)}(\beta\rho)}{(1-\eta^2)^{1/2}H_2^{(1)}(\beta)}\sin(\Omega\xi\eta)\,d\eta + \int_1^\infty \frac{\eta K_1(\gamma\rho)}{(\eta^2-1)^{1/2}K_2(\gamma)}\sin(\Omega\xi\eta)\,d\eta\right]e^{-i\Omega\tau}. \tag{28b}$$

The formal solution to the problem is expressed by the integral representations of eqns (26) and (28). These integrals will be integrated numerically since any attempt to integrate in the complex plane using residue theory would, in any case, lead to a numerical integration of the resulting branch integrals which are due to the multi-valued character of the Hankel functions. However special care must be given to the point $\eta = 1$ since it is observed here that $\beta \to 0$, $\gamma \to 0$ and that $\lim_{x\to 0} K_n(x) \to \infty$ and $\lim_{x\to 0} H_n(x) \to i\infty$.

Noting that for $|x| \ll 1$ [8],

$$K_1(x) \doteq 1/x, \qquad K_2(x) \doteq 2/x^2, \tag{29a, b}$$

it follows that

$$\lim_{\eta\to 1}\frac{K_1(\gamma\rho)}{\gamma K_2(\gamma)} = 1/(2\rho), \qquad \lim_{\eta\to 1}\frac{K_2(\gamma\rho)}{K_2(\gamma)} = 1/\rho^2. \tag{30a, b}$$

Identical results are obtained for equivalent ratios of the Hankel functions $H_n^{(1)}$ as $\eta \to 1$. Thus all the integrands appearing in eqns (26) and (28) are continuous and bounded in $0 < \eta < \infty$.

Convergence of the integrals as $\eta \to \infty$ and the method of integration are discussed in the Appendix.

It is of interest to note that, using eqns (23) and eqns (13) and the relations of eqn (24), the solution degenerates to the static response as $\Omega \to 0$:

$$v(\rho, \xi) = -\frac{P}{\mu\pi}\int_0^\infty \frac{K_1(\alpha\rho)}{\alpha K_2(\alpha)}\cos\alpha\xi\,d\alpha \tag{31a}$$

$$\sigma_{r\theta}(\rho, \xi) = \frac{P}{a\pi}\int_0^\infty \frac{K_2(\alpha\rho)}{K_2(\alpha)}\cos\alpha\xi\,d\alpha \tag{31b}$$

$$\sigma_{\theta z}(\rho, \xi) = \frac{P}{a\pi}\int_0^\infty \frac{K_1(\alpha\rho)}{K_2(\alpha)}\sin\alpha\xi\,d\alpha. \tag{31c}$$

These expressions are seen to be identical to those given in [6].

4. NUMERICAL RESULTS

Numerical results for the displacements and stresses are obtained from eqns (26) and (28) respectively using the scheme as described in the Appendix. It is noted however, that the first right-hand integrals containing the H_n functions which appear in these equations are complex quantities while the remaining integrals containing the K_n functions, are real. Consequently, the displacement and stress components have the form:

$$\mu v/P = [A + iB]e^{-i\Omega\tau}, \qquad a\sigma_{ij}/P = [C_{ij} + iD_{ij}]e^{-i\Omega\tau} \tag{32a, b}$$

where A, B, C_{ij} and D_{ij} are real numbers dependent on ρ, ξ and Ω.

Significant results for this steady state solution are therefore given in terms of the amplitudes $\mu|v|/P$ and $a|\sigma_{ij}|/P$.

Numerical results for the displacement amplitudes $|v|$ and the non vanishing stress component $|\sigma_{r\theta}|$ along the radial line $\xi = 0$ are presented in Figs. 2 and 3 as a function of the radial distance ρ for a relatively low value of Ω, $\Omega = 2$, and for a large value, $\Omega = 10$. (Results were obtained, using the scheme described in the Appendix, to 3 place accuracy for $\rho > 1.1$. For points $\rho < 1.1$ in the vicinity of the load, results of lesser accuracy were obtained, and the curves are therefore shown as broken lines.) The displacements and stresses are observed, as expected, to be very large in the neighbourhood of the applied load and to decay rapidly with increasing ρ. It is of interest to note that v is larger for the smaller value of Ω while the opposite is true for the stress component $\sigma_{r\theta}$. This feature is explained below.

The displacement along the bore surface, as a function of ξ is shown in Fig. 4, where, again, the displacement is seen to decay monotonically with the distance from the point

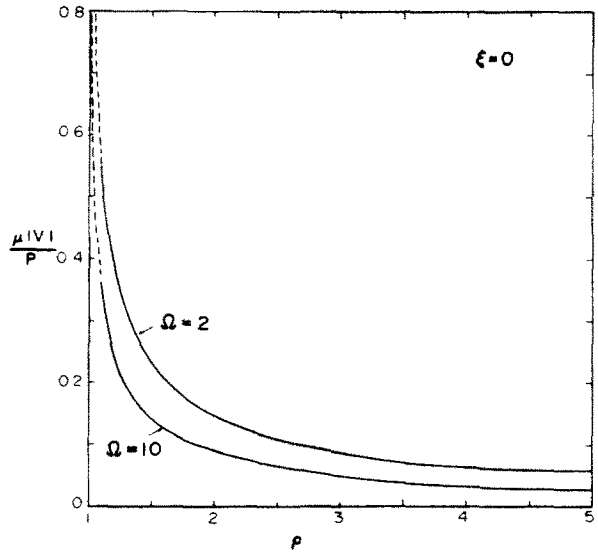

Fig. 2. Radial distribution of displacement $|v|$.

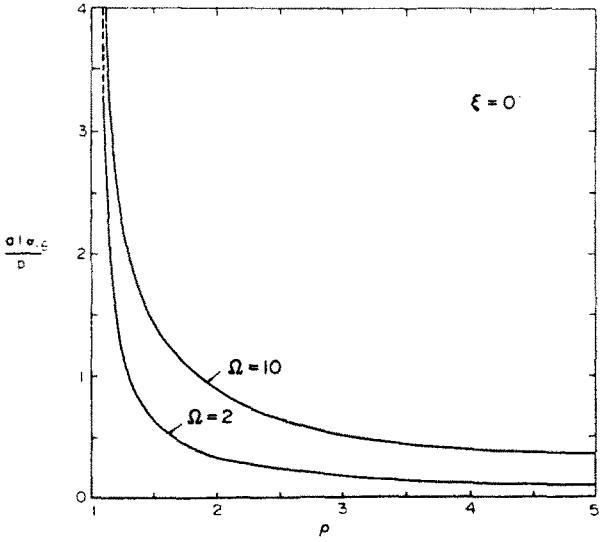

Fig. 3. Radial distribution of stress $|\sigma_{r\theta}|$.

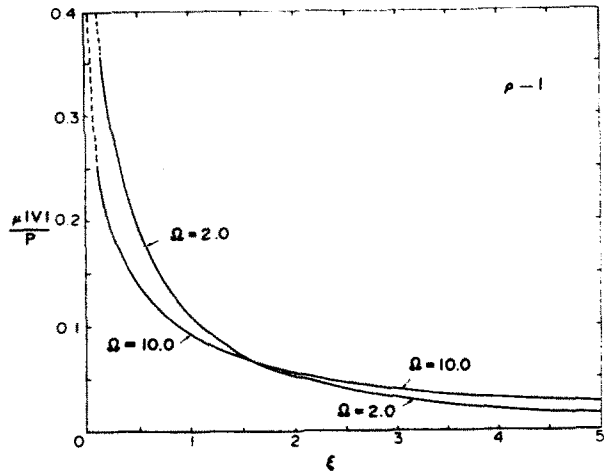

Fig. 4. Displacement variation along Bore Surface.

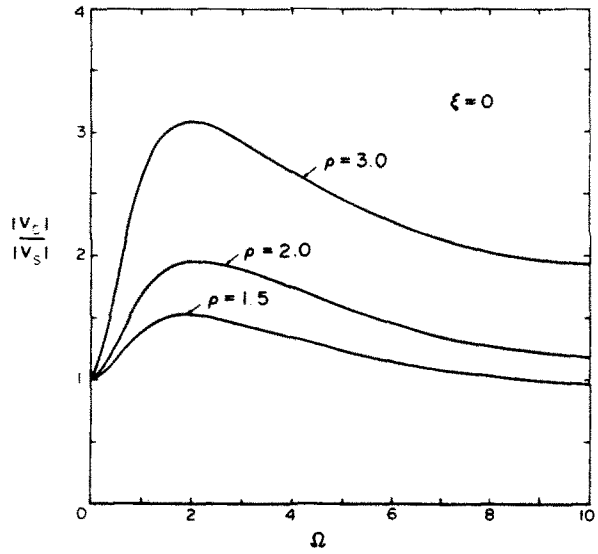

Fig. 5. Dynamic displacement amplification factors.

of load application.† The non-vanishing stress component $|\sigma_{\theta z}|$ displays a similar behavior and consequently the results are not repeated here. It is interesting to note, however, that while the decay with ξ is more rapid for larger frequencies in the region of the load, far away, i.e. for $\xi > 2$, these frequencies produce larger displacements.

A point of major interest is to compare the dynamic behavior with the corresponding static-behavior as given in [6]. The spatial distribution is observed to be roughly the same with a sharp monotonic decay with the distance away from the point of load application. However, quantitatively, we may examine the ratio of the dynamic to static response, $|v_D/v_s|$, for the displacement and $|\sigma_{r\theta,D}/\sigma_{r\theta,s}|$ for the stress-component along the radial line $\xi = 0$, i.e. the effective dynamic amplication factors. (The static quantities v_s and $\sigma_{r\theta,s}$ are obtained from [6].)

In Fig. 5, $|v_D/v_s|$ is presented as a function of the non-dimensional frequency Ω for three values of ρ: $\rho = 1.5$, 2.0 and 3.0. It is observed that the ratios start at $\Omega = 0$ from unity, reach a peak in the vicinity of $\Omega \sim 2$, and decrease with increasing values of Ω. The amplification factors are observed to increase with larger values of ρ; thus the effective penetration of the response is amplified greatly due the the application of harmonic forces.

†Results along the bore surface were calculated for $\rho = 1 + \epsilon$, ($\epsilon \ll 1$), rather then for $\rho = 1$ due the convergence problems when $\rho = 1$. (Such problems occur, as may be seen from eqns (A5b) and (A8), since $h = 0$ when $\rho = 1$.) Results were obtained for increasingly small values of ϵ and were seen to converge.

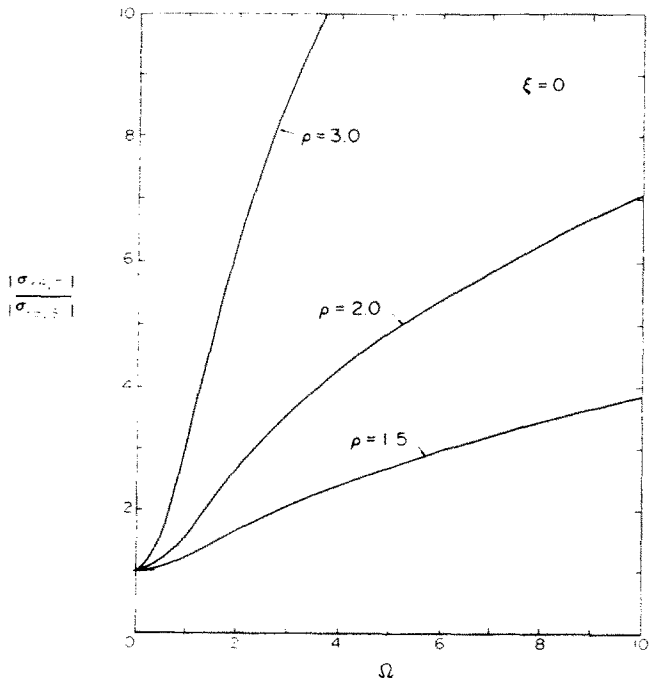

Fig. 6. Dynamic stress amplification factors.

The amplification factors, $|\sigma_{r\theta,D}/\sigma_{r\theta,S}|$, are shown in Fig. 6 for the same values of ρ. Here we observe that these factors do not reach a peak but instead increase monotonically with Ω. Again the dynamic effect is greatest for increasing ρ. From the results of Fig. 6, we may now reexamine results for Figs. 2 and 3 and understand why the effects due to $\Omega = 2$ and $\Omega = 10$ are inverted. Clearly, for the stresses, relatively large values of Ω will produce higher stresses while greater displacements will occur at frequencies in the neighborhood of the peak of Fig. 5.

5. DISCUSSION AND CONCLUSION

The spatial distributions of the displacement and stress components due to the application of time-harmonic tractions do not differ in form with those of the corresponding static case: amplitudes of large magnitude occur near the point of load application and decay monotonically with the distance from the load.

Of particular interest in the results given above and which merits explanation, is the fact that the dynamic effect as represented by the amplification factors, becomes stronger with larger values of ρ; i.e. the dynamic effect causes the significant radial penetration of the response to increase. To exaplain this requires a closer examination of the relevant equations; in order to arrive at a physical interpretation of the results it is in fact necessary to consider the propagation of waves in the medium.

From eqn (26), we observe that the expression for the displacement can be written as:

$$\mu v/P = \frac{1}{\pi}\left\{\int_0^{\Omega} F[H_n^{(1)}(\beta\rho)]\cos\alpha\xi\,\mathrm{d}\alpha + \int_{\Omega}^{\infty} G[K_n(\gamma\rho)]\cos\alpha\xi\,\mathrm{d}\alpha\right\}\mathrm{e}^{-i\Omega\tau} \tag{33}$$

where F and G represent symbolically the given functions of H_n and K_n respectively and where β and γ are real.

First, we note that the terms $\cos\alpha\xi\,\mathrm{e}^{i-\Omega\tau}$ represent the propagation of waves of wavelength

$$\lambda = 2\pi a/\alpha \tag{34}$$

which propagate in the z-direction with an apparent (phase) velocity $C_z = f\lambda$ (where f is the forcing frequency).

The integrals can then, as far as the z-direction is concerned, be considered as the sum of wave contributions of varying wave lengths from $\lambda = \infty$ ($\alpha = 0$) to $\lambda = 0$ ($\alpha \to \infty$).† We examine each integral in turn.

In the first integral, $\alpha < \Omega$. Using the definition given by eqn (11), this implies that $C_z/C_s > 1$. Thus the first integral represents waves of wavelength $\lambda > C_s/f$ which propagate with velocity $C_z > C_s$ in the z-direction. Expressing the $H_n^{(1)}$ functions appearing in the first integral by the first term of the asymptotic expansion[8], we note that

$$H_1^{(1)}(\beta\rho)\,e^{-i\Omega\tau} \sim \frac{1}{(\beta\rho)^{1/2}}\,e^{i(\beta\rho-\Omega\tau)} \tag{35}$$

and thus observe that this integral represents also outward radially propagating waves which decay as $\rho^{-(1/2)}$.

On the other hand, the second integral containing the K_n functions does not represent waves which propagate in the ρ direction but merely an exponentially decaying displacement pattern (see eqns 31)

These observations now permit us to explain the phenomenon of increasing radial penetration due to the dynamic effect. It has been previously observed that the static response, given by eqn (31) is represented solely by integrals containing K_n functions which, as has just been noted, describe non-propagating exponentially decaying displacement patterns. Consequently since the static response for relatively large values of ρ is necessarily small, it follows that the corresponding dynamic response, consisting partially of radiating waves (which decay only as $\rho^{-(1/2)}$), will necessarily always produce amplification factors which increase with the radial distance ρ.

REFERENCES

1. H. M. Westergaard, *Karman Anniversary Volume* (1941).
2. C. J. Tranter, On the elastic distortion of a cylindrical hole by a localised hydrostatic pressure. *Quart. Appl. Math.* **4**, 298–302 (1946).
3. D. W. Jordan, The stress wave from a finite cylindrical explosive source. *J. Math. Mech.* **11**, 503–551 (1962).
4. R. Parnes, Response of an infinite elastic medium to travelling loads in a cylindrical bore. *J. Appl. Mech.* **36**, 51–58 (1969).
5. R. Parnes, Progressing torsional loads along a bore in an elastic medium. *Int. J. Solids Structures* **16**, 653–670 (1980).
6. R. Parnes, Applied tractions on the surface of an infinite cylindrical bore. *Int. J. Solids Structures* **19**, 165–177 (1983).
7. I. N. Sneddon, *Fourier Transforms*. McGraw-Hill, New York (1951).
8. N. W. McLachlan, *Bessel Functions for Engineers*. Oxford (1955).

APPENDIX

Evaluation of the integrals appearing in eqns (26) *and* (28)

The right-hand integrals appearing in eqns (26) and (28) must be integrated over the infinite domain $1 \leqslant \eta < \infty$. Recognizing that the integrands represent ratios of the K_n functions, a prescribed value $\eta = \eta_0$ is chosen such that the infinite range is separated into two regions: $1 \leqslant \eta < \eta_0$ and $\eta_0 \leqslant \eta < \infty$. In the latter region the integrals can be integrated asymptotically by making use of the asymptotic relations for K_n. To this end let the various integrals be written as

$$S_{n,k} = S_{n,k}^{(1)} + S_{n,k}^{(2)} \tag{A1}$$

where

$$S_{n,k}^{(1)} = \int_1^{\eta_0} \chi_{n,k}(\eta,\rho)\begin{Bmatrix}\cos(\Omega\xi\eta)\\ \sin(\Omega\xi\eta)\end{Bmatrix} d\eta; \qquad S_{n,k}^{(2)} = \int_{\eta_0}^{\infty} \chi_{n,k}(\eta,\rho)\begin{Bmatrix}\cos(\Omega\xi\eta)\\ \sin(\Omega\xi\eta)\end{Bmatrix} d\eta \tag{A2a, b}$$

In the above,

$$\chi_{n,k}(\eta,\rho) = \frac{\eta^k K_n(\gamma\rho)}{(\eta^2-1)^{(2-n)/2}K_2(\gamma)}; \qquad n = 1, 2; \qquad k = 0, 1. \tag{A3}$$

†We note in passing that the second integral of eqn (33) represents the contribution of waves of decreasing wave lengths and which lead to the high value of v occurring in the neighborhood of the applied load.

The finite integrals $S_{n,k}^{(1)}$ are then integrated by an appropriate numerical scheme (e.g. Simpson's method). If x is chosen sufficiently large, then $K_n(x)$ can be represented by[8]

$$K_n(x) \sim \sqrt{(\pi/2x)}\, e^{-x}[1 + a_n/x + b_n/x^2 + \cdots] \tag{A4a}$$

where

$$a_n = \frac{4n^2 - 1}{8}, \qquad b_n = \frac{(4n^2 - 1)(4n^2 - 9)}{128}. \tag{A4b}$$

Using these asymptotic expansions and retaining the first few terms, the asymptotic representation of $\chi_{n,k}$ valid for $\eta_0 - 1 \gg 1/\Omega$ are immediately determined. The integrals $S_{n,k}^{(2)}$ may then be evaluated analytically or an upper bound of the value of $S_{n,k}^{(2)}$ may be established. Performing the integrations, the final results are given as follows:

$$\frac{\mu v(\rho, \xi)}{P} = -\frac{1}{\pi}[S_v^{(1)} + S_v^{(2)}]\, e^{-\Omega\tau} \quad (n = 1, k = 0) \tag{A5a}$$

where

$$S_v^{(2)} < \left| \frac{\rho^{-(1/2)} e^{-h}}{\Omega\Lambda(\eta_0^2 - 1)^{1/2}} \{(\rho - 1)\cos(\Omega\xi\eta_0) - \xi \sin(\Omega\xi\eta_0)\} \right|; \tag{A5b}$$

$$\frac{a\sigma_{r\theta}}{P}(\rho, \xi) = \frac{\Omega}{\pi}[S_{r\theta}^{(1)} + S_{r\theta}^{(2)}]\, e^{-\Omega\tau} \qquad (n = 2, k = 0), \tag{A6a}$$

where

$$S_{r\theta}^{(2)} < \left| \frac{\rho^{-(1/2)}}{\Lambda} e^{-h} \{(\rho - 1)\cos(\Omega\xi\eta_0) - \xi \sin(\Omega\xi\eta_0)\} \right|; \tag{A6b}$$

$$\frac{a\sigma_{\theta z}}{P}(\rho, \xi) = \frac{\Omega}{\pi}[S_{\theta z}^{(1)} + S_{\theta z}^{(2)}]\, e^{-\Omega\tau} \quad (n = 1, k = 1), \tag{A7a}$$

where

$$S_{\theta z}^{(2)} < \left| \frac{\rho^{-(1/2)}}{\Lambda} \left\{ \frac{(\eta_0 - 1)^{1/2}\Omega + 1}{(\eta_0 - 1)^{1/2}\Omega} \right\} e^{-h} \{(\rho - 1)\sin(\Omega\xi\eta_0) + \xi \cos(\Omega\xi\eta_0)\} \right|. \tag{A7b}$$

In the above

$$h = (\rho - 1)(\eta_0 - 1)\Omega, \qquad \Lambda = (\rho - 1)^2 + \xi^2. \tag{A8}$$

It is observed that an upper bound has been established on the remainders thus demonstrating the convergence of the integrals for all $\rho > 1$. An appropriate choice of η_0 will then give a prescribed accuracy to the solution.